Supplementary Materials for

Evolution of Ocean Temperature and Ice Volume Through the Mid-Pleistocene Climate Transition

H. Elderfield,* P. Ferretti, M. Greaves, S. Crowhurst,
I. N. McCave, D. Hodell, A. M. Piotrowski

*To whom correspondence should be addressed. E-mail: he101@cam.ac.uk

Published 10 August 2012, *Science* **337**, 704 (2012)
DOI: 10.1126/science.1221294

This PDF file includes:

Other Supplementary Materials for this manuscript include the following:
(available at www.sciencemag.org/cgi/content/full/337/6095/704/DC1)

Tables S1 to S3 as Excel files

Supplementary Materials

Materials and Methods

Material and methods for analyses of stable O and C isotopes and Mg/Ca of foraminifera

The methodology in this paper is based on the recognition that analysis of the oxygen isotopic composition of benthic foraminiferal calcite provides a means of estimating changes in deep ocean temperature and ice volume through geological time (Fig. S1). The methodology followed work carried out previously (*15*) on the upper part of core ODP 1123 from the Chatham Rise S.E. of New Zealand, information on which is shown in Fig. S2. The majority of the isotope measurements on *Uvigerina* spp. reported here were made on a Micromass multicarb sample preparation system attached to a PRISM mass spectrometer, and were supplemented where necessary with data previously published (*45*). Measurements were determined relative to the Vienna Peedee Belemnite (VPDP) Standard with an analytical precision of ± 0.08‰ for $\delta^{18}O$ and 0.06‰ for $\delta^{13}C$. Mg/Ca analyses were carried out following the cleaning procedure described in (*48*) and element ratios determined by ICP–OES (*49*) and ICP-MS (*50*). Long-term instrumental precision of element ratio data, determined by replicate analyses of a standard solution containing Mg/Ca = 1.3 mmol/mol, was ±0.46%. Accuracy of Mg/Ca determinations was confirmed by interlaboratory studies of foraminifera and carbonate reference materials (*51,52*).

Evaluation of data quality

Mg/Ca results (together with those for $\delta^{18}O$) are shown in Fig. 1 and listed in Table S1. A more detailed presentation of data are available at doi:10.1594/PANGAEA.786205. Results from 21 duplicate pairs of Mg/Ca analyses, 20 of which are from the same depths in the working and archive halves of the core, are given in Table S2. The pooled standard deviation of the duplicate Mg/Ca determinations is 0.055 mmol/mol, equivalent to an overall average precision of 5.4% including artefacts from cleaning, picking and sample heterogeneity in addition to instrumental precision.

Fe/Ca and Mn/Ca were measured to monitor cleaning efficiency and diagenetic effects. Fe/Ca was < 0.1 mmol/mol on all except 15 of the 1,485 analyses with no trend versus Mg/Ca ($r = 0.143$ $p < 0.0001$). Mn/Ca increases down-core ranging from 0.01 mmol/mol at the core-top to 0.36 mmol/mol at 1,435 ka (Fig. S13). Near the top of the core there is no significant correlation between Mg/Ca and Mn/Ca (*15*) but correlation becomes statistically significant for samples older than ~130 ka ($r = 0.403$, $p < 0.0001$) where some features visible in the Mg/Ca record are also seen in the Mn/Ca record. This similarity between the records probably reflects climate related diagenetic reorganisation of Mn rather than an imprint affecting Mg. Assuming an Mg/Mn ratio of 0.1 mol/mol within a diagenetic coating, consistent with Mg/Mn ratios found in manganese nodules and micro-nodules (*53,54*) and manganese carbonate in marine sediments (*55*), would imply a maximum contribution of 0.04 mmol/mol to Mg/Ca in this record, within the reproducibility found from duplicate analyses.

Twelve of the samples were found to have low Mg/Ca ratios (< 0.75 - 0.8 mmol/mol) and thus very cold temperatures predicted via the Mg/Ca temperature sensitivity used (Table S3).

These were most obvious in MIS 42 and 46. The lowest Mg/Ca ratios found in MIS 46 were associated with anomalously heavy specimens, weighing on average 38 μg compared to typically 26 μg over most of the record. It seems likely that these low Mg/Ca ratios are a consequence of species variations. The low Mg/Ca samples (a cut off of 0.8 mmol/mol is used) occur where abundances of the hispid and unadorned species of *Uvigerina* are high and where the costate and especially the hispidocostate spp. disappear (Fig. S14). Therefore, these low Mg/Ca ratio samples were not plotted in Fig. 1 and glacial data for MIS 42 and 46 are not used.

Age models for Core ODP 1123

The age model for the core from ODP Site 1123 used here was obtained by tuning the *Uvigerina* spp. $\delta^{18}O$ data to the Lisiecki and Raymo $\delta^{18}O$ stack (*19*). The model is for the most part similar to the age model constructed by Hall et al. (*45*). Re-evaluation of the age model for isotope stages 34-49 has been carried out for this paper. The revised composite depth scale (r-mcd) developed by Hall et al (*45*), who added 2.72 m to cores 181-1123B-5H and 181-1123C-5H and deeper (*56*), was followed for evaluation of the age model in this work. More recently a repeated section in the 1123C core was identified (*57*) and we followed the advice to restrict sampling to the 1123B core between ~41.0 and 54.0 mbsf to obtain an undisturbed record.

Conversion of foraminiferal Mg/Ca to temperature

Foraminiferal Mg/Ca ratios are commonly used to estimate ocean temperature. It has been recognised recently that Mg/Ca ratios of epibenthic foraminifera are affected by carbonate saturation effects (*7,8*). In one recent record a "regional calibration" (i.e. sensitivity, S_{Mg}) of 0.15 mmol/mol per ºC was used to account for both temperature and carbonate saturation effects on benthic foraminiferal Mg/Ca (*6*). Previously we carried out a calibration study using the shallow-infaunal benthic foraminifera *Uvigerina* spp. showing that, because of its infaunal habitat, it is little affected by bottom water carbonate saturation (*15*). The 57 point core-top data used in that calibration are shown in Fig. S4A. Mg/Ca-T paired data have a Student t-test correlation probability <0.0001 correlation coefficient r = 0.90. However, some uncertainty exists over the most appropriate formulation of temperature sensitivity. Therefore, as in (*15*) we used S_{Mg} of 0.10 mmol/mol per ºC guided by its prediction of accurate values for glacial and interglacial temperature estimates over Marine Isotope Stages 2-1 (Fig. S4B).

Conversion of Mg/Ca and calcite $\delta^{18}O_C$ to seawater $\delta^{18}O_W$

Given Mg/Ca, combination of the linear version of the Mg thermometry equation ($Mg/Ca = m_1 + S_{Mg}T$) and the linear version of the paleotemperature equation ($T = m_2 - (\delta^{18}O_C - \delta^{18}O_W)/S_O$), m_1 and m_2 are constants, allows changes in the oxygen isotopic composition of seawater ($\Delta\delta^{18}O_W$) to be calculated from

$$\Delta\delta^{18}O_w = \Delta\delta^{18}O_C + \Delta Mg/Ca \frac{S_O}{S_{Mg}}$$

where S is the sensitivity of $\delta^{18}O_C$ and of Mg/Ca to temperature. This formulation shows it is the ratio of the sensitivity of both $\delta^{18}O_C$ and of Mg/Ca to temperature which defines $\Delta\delta^{18}O_W$. Exact "true equilibrium" values are not known either for Mg/Ca or $\delta^{18}O_C$, although commonly used values of S_{Mg} are as here ~0.1 mmol/mol per ºC and for S_O of ~ 0.25 ‰ per ºC. In Fig. S6 we show estimates of $\delta^{18}O_W$ made with 3 different combinations of S_O/S_{Mg}: 2.5 (from 0.25/0.1), 3.0 (from 0.3/0.1 or 0.25/0.08) and 2.0 (from 0.2/0.1 or 0.25/0.125).

Conversion of seawater $\delta^{18}O_W$ to sea level

Most sealevel estimates for paleoceanographic studies make simplifying assumptions in the conversion of oxygen isotope measurements of seawater as compared with ice sheet models. It has been shown that the inaccuracy from linearly inferring ice volume variations from $\Delta\delta^{18}O_W$ changes is mostly less than 10% (*27*). Assuming the difference between the mean isotopic composition of the ocean and the ice sheets does not change it is simple to explore the difference between $\delta^{18}O_W$ (δ_W) and sealevel fall (Z) for $\delta^{18}O$ of ice (δ_i):

$$\delta_W = \frac{-\delta_I Z}{D_O - Z}$$

where D_O is ocean depth (Fig. S7). Typically it is assumed that an increase in δ_W of 1 ‰ is equivalent to a sea level fall of either 100m (δi = -40 ‰) or 120m (δi = -32 ‰). Assumption of δ_W based on a constant δ_i has little impact on derivation of sea level estimated from δ_W records during the start of a glacial cycle but has a larger impact at full glaciation. Here we have used δ_i = -40 ‰.

Methods for Nd isotope analyses

Bulk sediment samples from ODP Site 1123 were wet sieved at 63 μm and the remaining course fraction was dry sieved to separate shells >250 μm. From this fraction ~20 mg mixed planktonic species were picked, crushed and their clays removed prior to dissolution in ~0.1 M acetic acid. Rare earth elements were separated from other elements using Eichrom TRUspec™ resin. Neodymium was then separated from REEs using Eichrom LNspec™ resin, on volumetrically calibrated columns. Neodymium isotopes of larger samples were analyzed by Nu Plasma HR multi-collector plasma mass spectrometer (MC–ICPMS) at the University of Cambridge, while smaller samples were obtained using a Thermo Finnigan Neptune MC-ICPMS at the Pôle Spectrométrie Océan (IFREMER, Brest, France). Mass fractionation was corrected by normalising $^{146}Nd/^{144}Nd$ to 0.7219 applying an exponential-fractionation correction, and each sample was bracketed with analyses of the JNDi-1 neodymium isotopic standard with a value of 0.512115 ±7 (*58*).

Supplementary text

The phase relationship of the Mg/Ca temperature record to orbital forcing: the temperature lag of eccentricity forcing

The Mg/Ca record of IODP Site 1123 highlights the important question of the relationship between orbital forcing, temperature and ice volume at eccentricity periodicities. Ruddiman (*59*) argued that "The 15,000-year lag of the 100,000-year ice-volume signal behind eccentricity proposed by Shackleton (*2*) makes no sense based on reliable evidence and must be rejected." The ODP1123-based Mg/Ca temperature record after the MPT presents these questions in a more direct form. The separated record of ice volume lags the Mg/Ca temperature change proxy by a significant amount (of the order of 21 ka) as predicted *(2),* but the record of temperature change within $\delta^{18}O$ on conventional isotope chronologies (such as the LR04 chronology) leads, not lags, its supposed orbital pacing by conventionally expressed orbital eccentricity. Rather than reject the hypothesis of the eccentricity pacing of temperature change, we suggest that the phase relationship between two powerful components of the orbital forcing at 100 ka periodicities may be responsible. The changes in warm season insolation intensity caused by changes in the Earth's proximity to the sun at perihelion (Curve A, Fig. S15) are combined with warm season duration changes caused by the operation of Kepler's second law (Curve B, Fig. S15) which, though originally precisely inverse to the "conventional" eccentricity curve, are differentially lagged by the Earth's climate system response.

Combined at their original antiphase relationship, these two forcing curves would exactly cancel each other out. However, if one of the curves - the warm season extension curve represented by inverse eccentricity - is lagged by a significant amount, of the order of 25 ka, a very different pattern and phase relationship for the forcing emerges; and, more importantly for this discussion, explains the phase relationship between orbital forcing and the oceanic Mg/Ca record.

We suggest that the growth of very large ice sheets around the time of the MPT may have induced this delayed response to seasonal extension by the climate system and locked the planetary climate system into a tightly constrained 100 kyr periodicity. The total orbital forcing at eccentricity periods therefore represents a combination of both "conventional" eccentricity forcing by insolation intensity changes, and "inverse eccentricity" changes caused by warm season extension. Lisiecki (*60*) has already highlighted the potential role of inverse eccentricity in orbital forcing, though with a different mechanism of operation.

Figure legends S1 to S15

Figure S1 Cartoon showing methodology of separating temperature and seawater $\delta^{18}O$ components of benthic foraminiferal $\delta^{18}O$. As explained in the text, $\delta^{18}O$ of sea water is related to continental ice volume and hence to sea level. This requires some approximations for conversion as shown in Fig. S4-7.

Figure S2 Basic hydrography and location of ODP 1123 on Chatham Rise. **A** N-S salinity profile on WOCE line P15 showing Lower Circumpolar Deep Water with a maximum S >34.73 at the depth of core site ODP 1123; **B** Map of the region east of New Zealand showing the location of ODP 1123 on Chatham Drift in relation to deep flow paths and sediment supply routes (Solander (SC), Bounty (BC) and Hikurangi (HC), path of the deep western boundary current (DWBC); ACC, Antarctic Circumpolar Current; CVZ, central volcanic zone; HP,

Hikurangi Plateau (after (*17, 45*)); **C** Hydrographic profiles from Valerie Passage (station R631, 41°S, 167°W) showing features of the main water masses including Antarctic Intermediate Water (AAIW), North Pacific Deep Water/Upper Circumpolar Deep Water (NPDW/UCDW), Lower Circumpolar Deep Water (LCDW) (which contains a salinity maximum indicative of North Atlantic Deep Water (NADW)) (after (*17, 45*)).

Figure S3 A Comparison of benthic $\delta^{18}O$ of LR04 stack with ODP 1123 $\delta^{18}O$ record derived from *Cibicidoides wuellerstorfi* and *Uvigerina* spp. and corrected by 0.64 (‰) offset from *Cibicidoides*. Benthic $\delta^{18}O$ records of ODP 1123 compared with **B** ODP 677 (*61*), 846 and 849 (*62*) from east equatorial Pacific Ocean, **C** ODP 1090 from south Atlantic Ocean (*63*), and **D** ODP 1308 from north Atlantic Ocean (*64*).

Figure S4 A Mg/Ca of *Uvigerina* spp compared with bottom water temperatures of core-top sampling sites; after ref. (*15*). Core-top samples for calibration purposes that cover the coldest temperatures expected for glacial-age foraminifera are not readily available (black arrows show Last Glacial Maximum LGM and modern Bottom Water Temperature BWT) for ODP 1123. For this reason we carried out a sensitivity analysis - fig. **B** - comparing temperature change based on different values of temperature sensitivity (S_{Mg} of 0.12 – 0.07 mmol/mol per ºC) with glacial temperature (-1.2 ± 0.5 ºC) derived from porewater analysis (*26*) minus Holocene (5ka) temperature of +1.3 ±0.5 ºC) in blue. Note that porewater analysis was carried out using the same ODP core as used in this work. Values of glacial and of Holocene temperature are shown in grey and placed at 6 ka for comparison. The glacial minus Holocene Δtemperature is shown in red and placed at 18 ka for comparison with estimates of Δtemperature.

Figure S5 Comparison of ODP1123 temperatures from this work and ice-core temperatures from (*16*). Temperature $\delta D = -6.1 \pm 0.08 + 2.10 \pm .08$ $temperature_{Mg}$ ($r=0.67$). The regression has a similar slope to that found from a comparison of ice-core and global temperatures (*23*).

Figure S6 Comparison of sea level estimates from coral reefs with seawater $\delta^{18}O$ derived from ODP 1123 records assuming 1‰ $\delta^{18}O$ equivalent to 100m sea level (see Fig. S7). **A** coral data from (*24,25*), red squares, and $\delta^{18}O$ (blue line) based on ratio of sensitivity to temperature of benthic $\delta^{18}O$ to that of Mg/Ca (S_O/S_{Mg}) of 2.5. **B** coral data (red line) and three estimates of sensitivity ratio S_O/S_{Mg} 2.5 (blue), 3 (purple) and 2 (brown). **C** coral data (red line), sea level from Red Sea (28) and simulation (*11*). Right hand ordinate scale is of sea level (m) assuming 1‰ change in $\delta^{18}O_W$ is equivalent to 100 m of sea level change.

Figure S7 Relationship between $\delta^{18}O$ of seawater (δW) and sea level Z (km) for different values of $\delta_{18}O$ of ice (δI). DO is oceanic depth, assumed 4.0 km, in simple numerical calculation. The commonly used values of 1‰ change in δW as equivalent to 100m of sea level change, or 12‰ equivalent to 120m (in red), imply $\delta I = -40$‰ as used here.

Figure S8 Histogram showing $\Delta\delta_W$ (blue) and $\Delta\delta_T$ (red) versus Marine Isotope Stage (MIS). Horizontal blue lines show averages for glacials at eccentricity (MIS 2-24) $\Delta\delta_W = 1.09 \pm 0.17$ and

obliquity (MIS 24-50) $\Delta\delta_W = 0.72 \pm 0.17$. Temperature values show no trend: $\Delta\delta_T = 0.74 \pm 0.08$ for MIS 2-22 and $\Delta\delta_T = 0.80 \pm 0.10$ for MIS 24-50, averaging 0.79 ± 0.11, equivalent to a cooling of 3.2 ± 0.4 ºC (assuming 0.25‰/ºC). The modern bottom water temperature at the site of ODP 1123 is 1.3 ºC, implying an average glacial temperature of -1.9 ± 0.4 ºC. The freezing point of surface water of salinity 36 (the estimated LGM salinity at Chatham Rise (*26*)) is -1.98 ºC.

Figure S9 Bandpass filtered data for ODP 1123. Eccentricity and Obliquity periodicities for Temperature Mg/Ca (red), $\delta^{18}O_C$ (black) and $\delta^{18}O_W$ (green) ; and $\delta^{13}C$ (blue) and $\delta^{18}O_W$(green).

Figure S10 Comparison of $\delta^{13}C$ of epifaunal *Cibicidoides* spp. and shallow infaunal *Uvigerina* spp. Data and line in red show crossplot of data that fits the equation *Uvigerina* $\delta^{13}C$ = *Cibicidoides* $\delta^{13}C$ -0.86 ($r^2 = 0.56$) consistent with offset of 0.9‰ between species. Data and line in blue shows crossplot where 0.9‰ added to *Cibicidoides* $\delta^{13}C$ yielding equation *Uvigerina* $\delta^{13}C$ = *Cibicidoides* $\delta^{13}C + 0.04$ ($r^2 = 0.56$)

Figure S11 Crosplots of $\delta^{13}C$ versus εNd for the 3 data sets shown in Figure 6 (MIS 1-2, 10-12 and 35-37). A value of 0.9 ‰ has been added to the *Uvigerina* spp. $\delta^{13}C$ as explained in the text (see also Fig. S10). **A** Data compared with mixing line after (*46*) for interglacial mixing between NADW and a Pacific end member. **B** Separation of data into vectors reflecting mixing (as in A) and change in benthic $\delta^{13}C$ reservoir (ie offset from mixing line independent of εNd). The coloured arrows through data are for illustration to indicate that the size of offset of $\delta^{13}C$ from εNd varies from 0.2 to 0.5‰.

Figure S12 Record over 700-1,250 ka showing age of initiation of the MPT at MIS 22 inferred from $\delta^{18}O_W$ (sealevel), (black) also showing ice-core CO_2 record (red) (*16*) and CO_2 based on $\delta^{11}B$ (red squares (*47*)).

Figure S13 Mg/Ca record of ODP 1123 compared with Mn/Ca record. As discussed in Material and Methods "Evaluation of data quality" it is unlikely that diagenetic ferromanganese coatings on foraminifera have had a significant effect on Mg/Ca ratios. Also shown is sedimentation rate derived from rmcd and LR04 age model. The main features which were avoided are the anomalous rates in intervals where cores are spliced.

Figure S14 Mg/Ca of *Uvigerina* species over range 1260-1470 ka LR04 (~59-65 revised meter composite depths r mcd) for hispid and unadorned species of *Uvigerina* (H) compared with costate species (C). Samples with high H/C ratios (and high H and low C) are associated with low Mg/Ca ratios (< 0.8 mmol/mol).

Figure S15 Comparison of curves showing in normalised data **A** eccentricity (blue), **B** inverse eccentricity lagged by 25 ka (red) and **C** combined eccentricity (black). ODP 1123 Mg/Ca is shown in red.

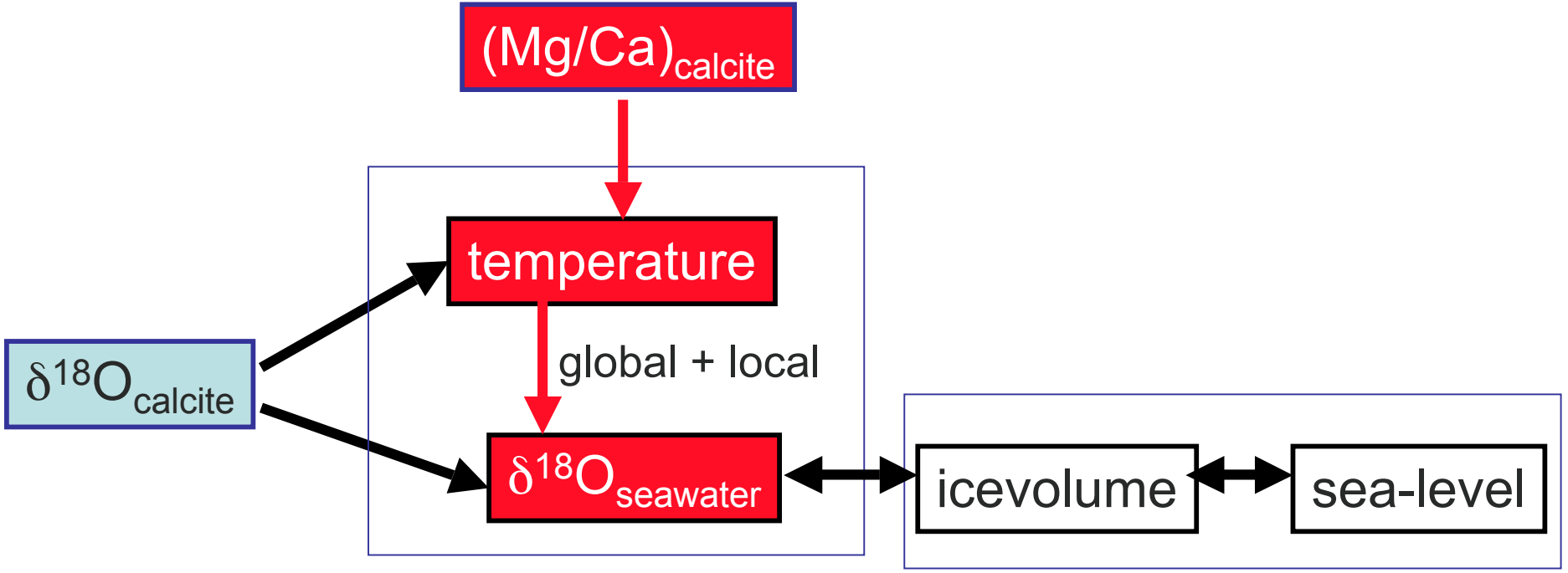
(Mg/Ca)calcite
temperature
global + local
δ18Ocalcite
δ18Oseawater
icevolume
sea-level

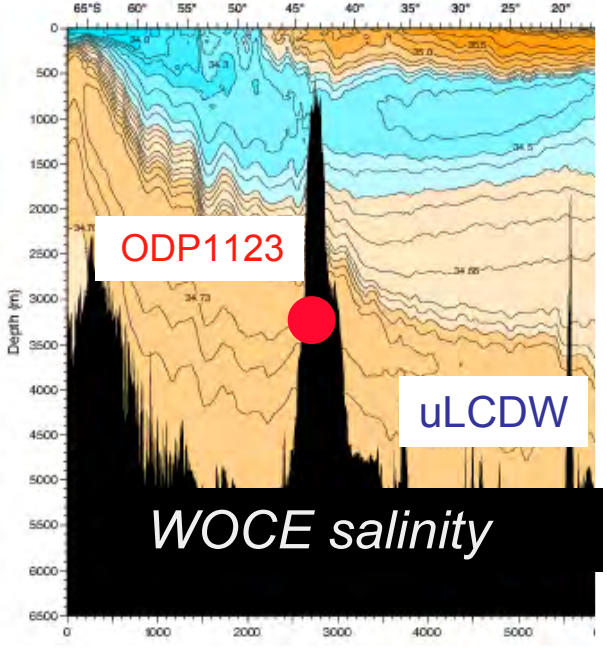
ODP1123
uLCDW
WOCE salinity
Depth (m)

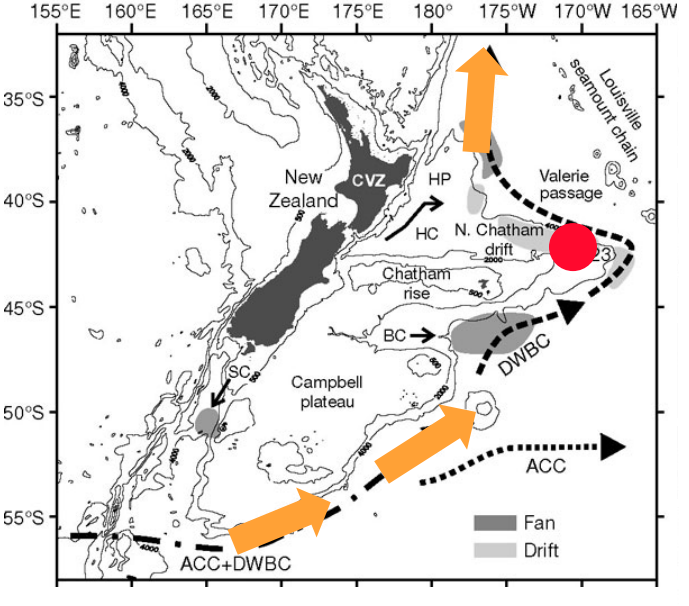
New Zealand
CVZ
HP
HC
N. Chatham drift
Chatham rise
Valerie passage
Louisville seamount chain
BC
DWBC
SC
Campbell plateau
ACC
ACC+DWBC
Fan
Drift

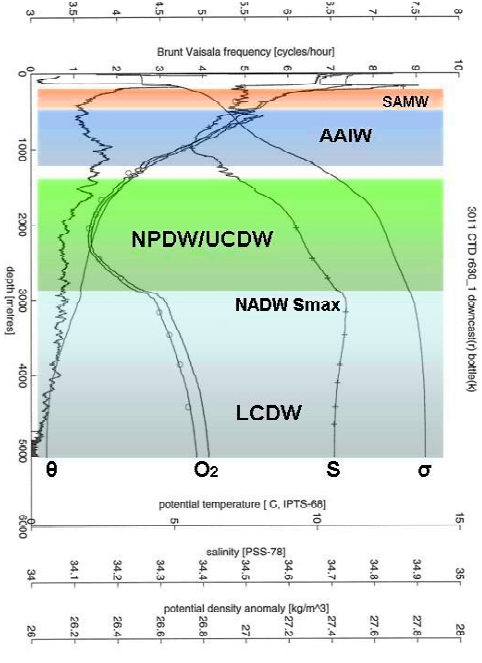
Brunt Vaisala frequency [cycles/hour]
SAMW
AAIW
NPDW/UCDW
NADW Smax
LCDW
θ
O2
S
σ
potential temperature [C, IPTS-68]
salinity [PSS-78]
potential density anomaly [kg/m^3]
2011 CTD 630_1 downcast(0) bottle(k)

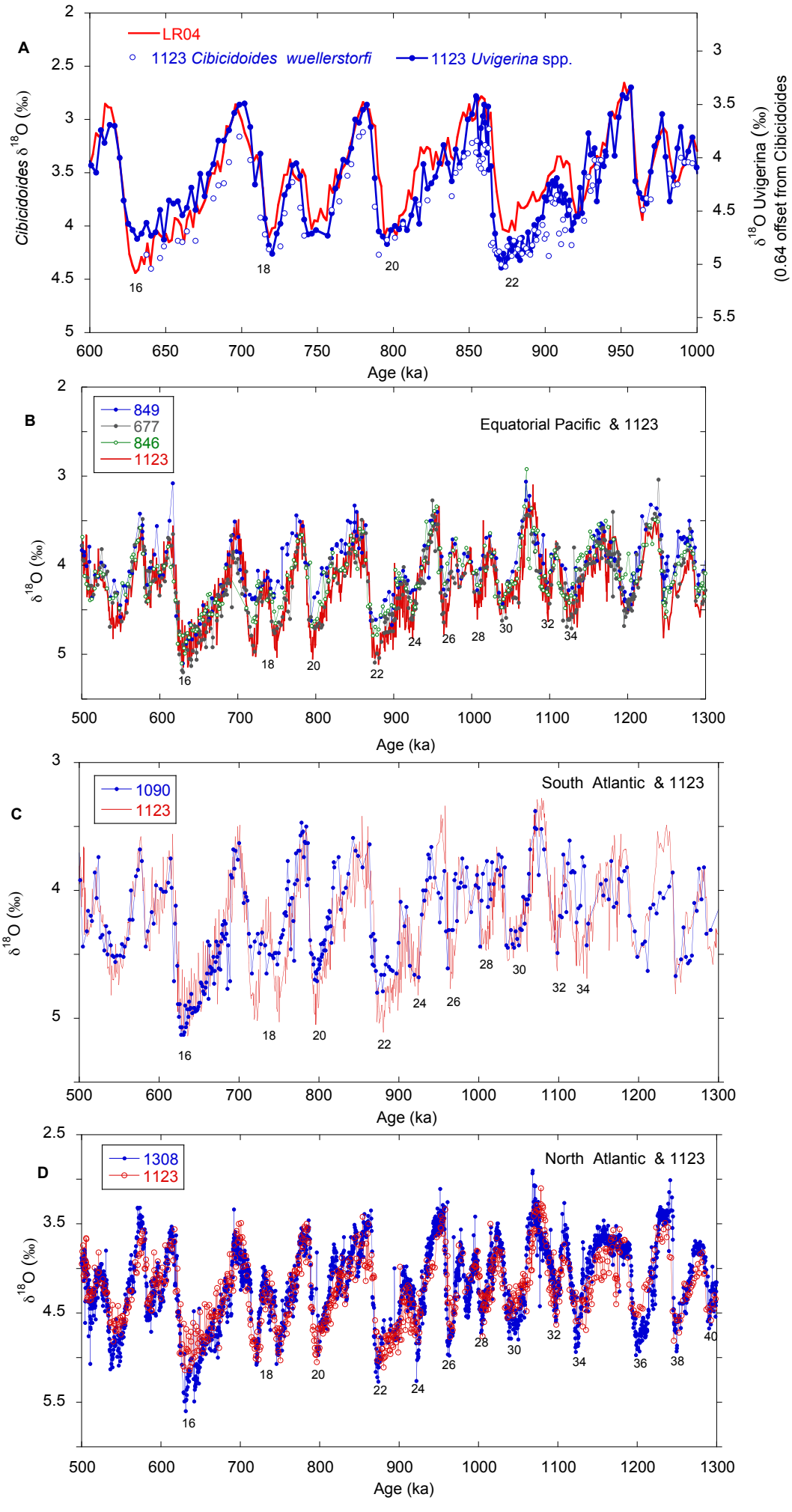
A
LR04
1123 Cibicidoides wuellerstorfi
1123 Uvigerina spp.
Cibicidoides δ18O (‰)
δ18O Uvigerina (‰)
(0.64 offset from Cibicidoides
Age (ka)
B
849
677
846
1123
Equatorial Pacific & 1123
δ18O (‰)
Age (ka)
C
1090
1123
South Atlantic & 1123
δ18O (‰)
Age (ka)
D
1308
1123
North Atlantic & 1123
δ18O (‰)
Age (ka)

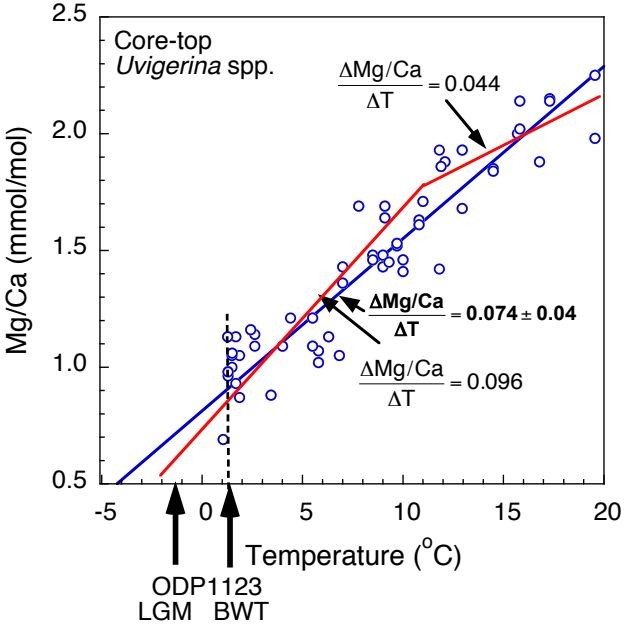
Core-top
Uvigerina spp.
ΔMg/Ca / ΔT = 0.044
ΔMg/Ca / ΔT = 0.074 ± 0.04
ΔMg/Ca / ΔT = 0.096
Mg/Ca (mmol/mol)
Temperature (°C)
ODP1123
LGM BWT

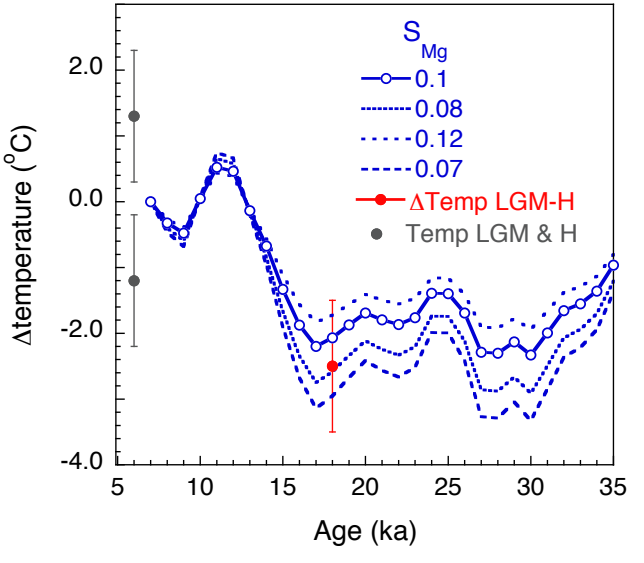
S Mg
0.1
0.08
0.12
0.07
ΔTemp LGM-H
Temp LGM & H
Δtemperature (°C)
Age (ka)

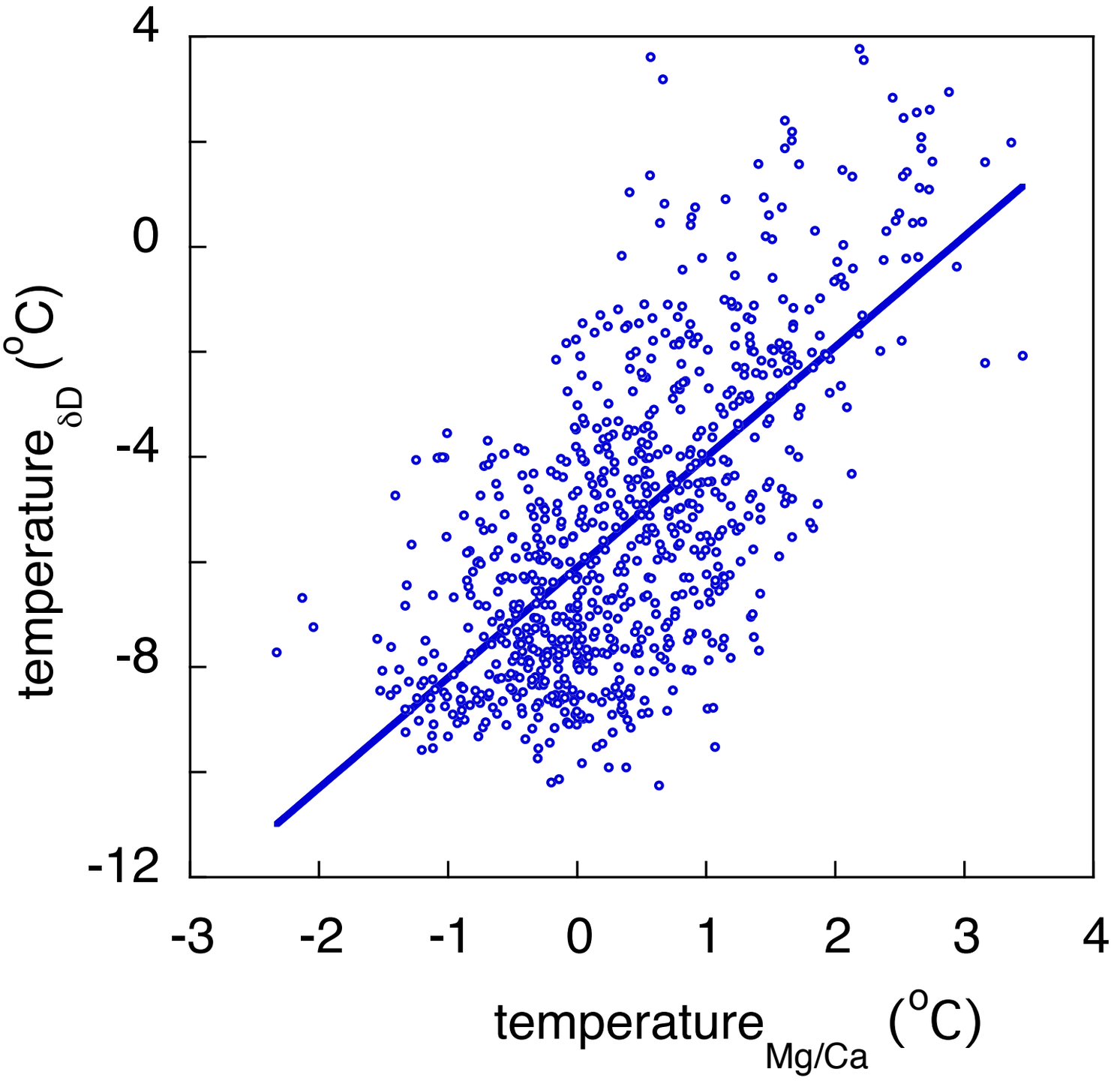
4
0
-4
-8
-12
-3
-2
-1
0
1
2
3
4
temperature$_{\delta D}$ (^{o}C)
temperature$_{Mg/Ca}$ (^{o}C)

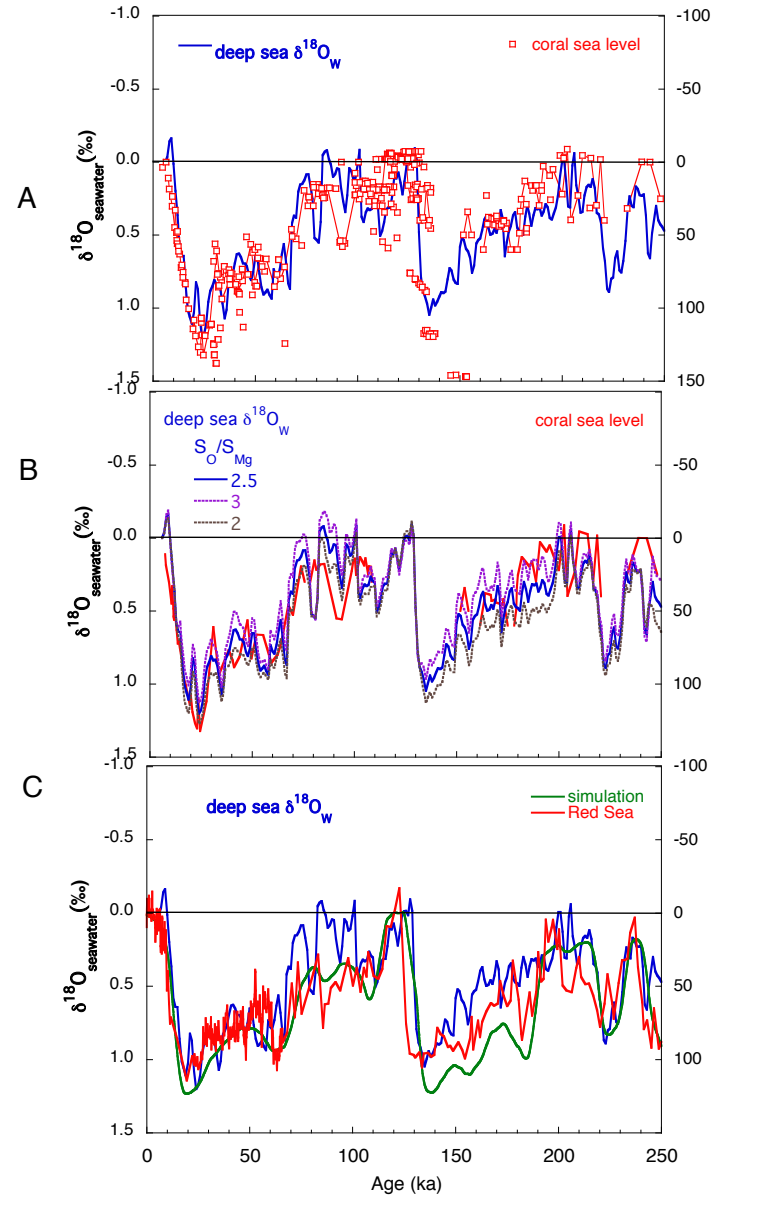
A
deep sea δ18Ow
coral sea level
δ18Oseawater (‰)
-1.0
-0.5
0.0
0.5
1.0
1.5
-100
-50
0
50
100
150
B
deep sea δ18Ow
coral sea level
So/SMg
2.5
3
2
C
deep sea δ18Ow
simulation
Red Sea
0
50
100
150
200
250
Age (ka)

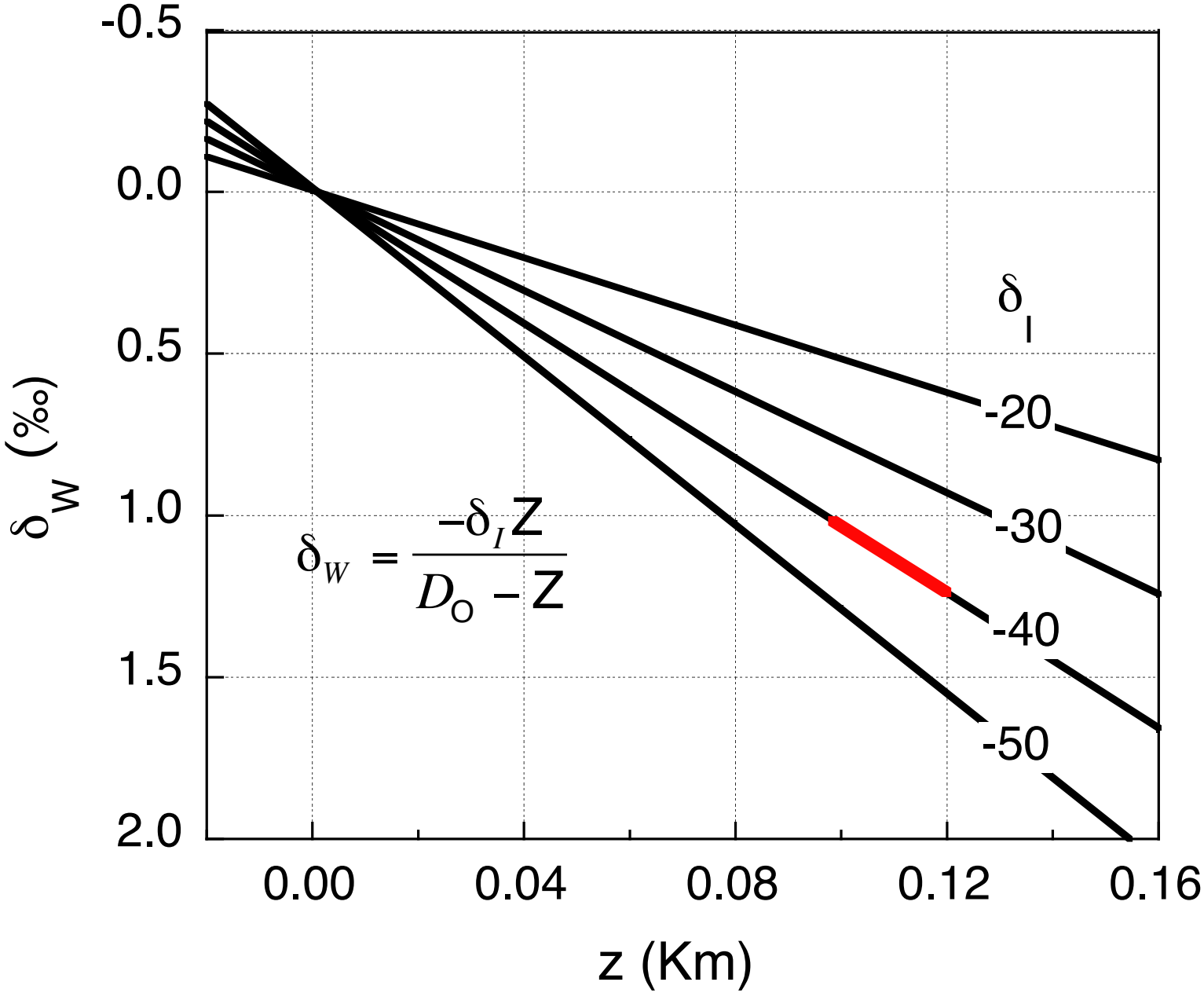
-0.5
0.0
0.5
1.0
1.5
2.0
δW (‰)
0.00
0.04
0.08
0.12
0.16
z (Km)
δI
-20
-30
-40
-50
δW = –δI Z / DO – Z

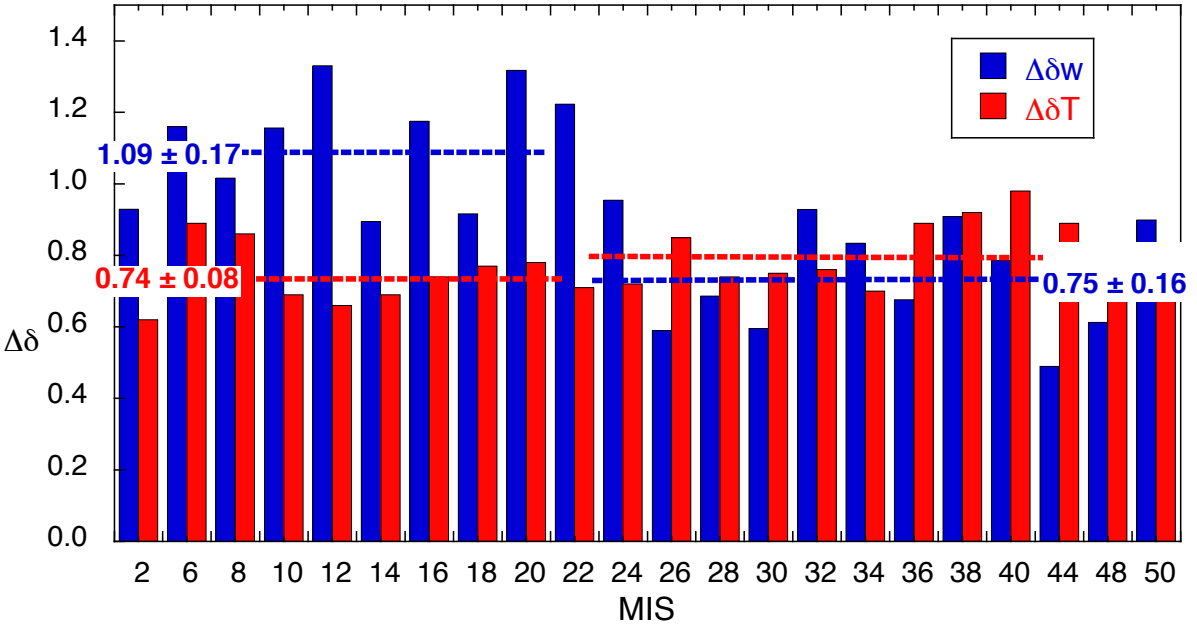
Δδw
ΔδT
1.09 ± 0.17
0.74 ± 0.08
0.75 ± 0.16
Δδ
MIS
0.0
0.2
0.4
0.6
0.8
1.0
1.2
1.4
2
6
8
10
12
14
16
18
20
22
24
26
28
30
32
34
36
38
40
44
48
50

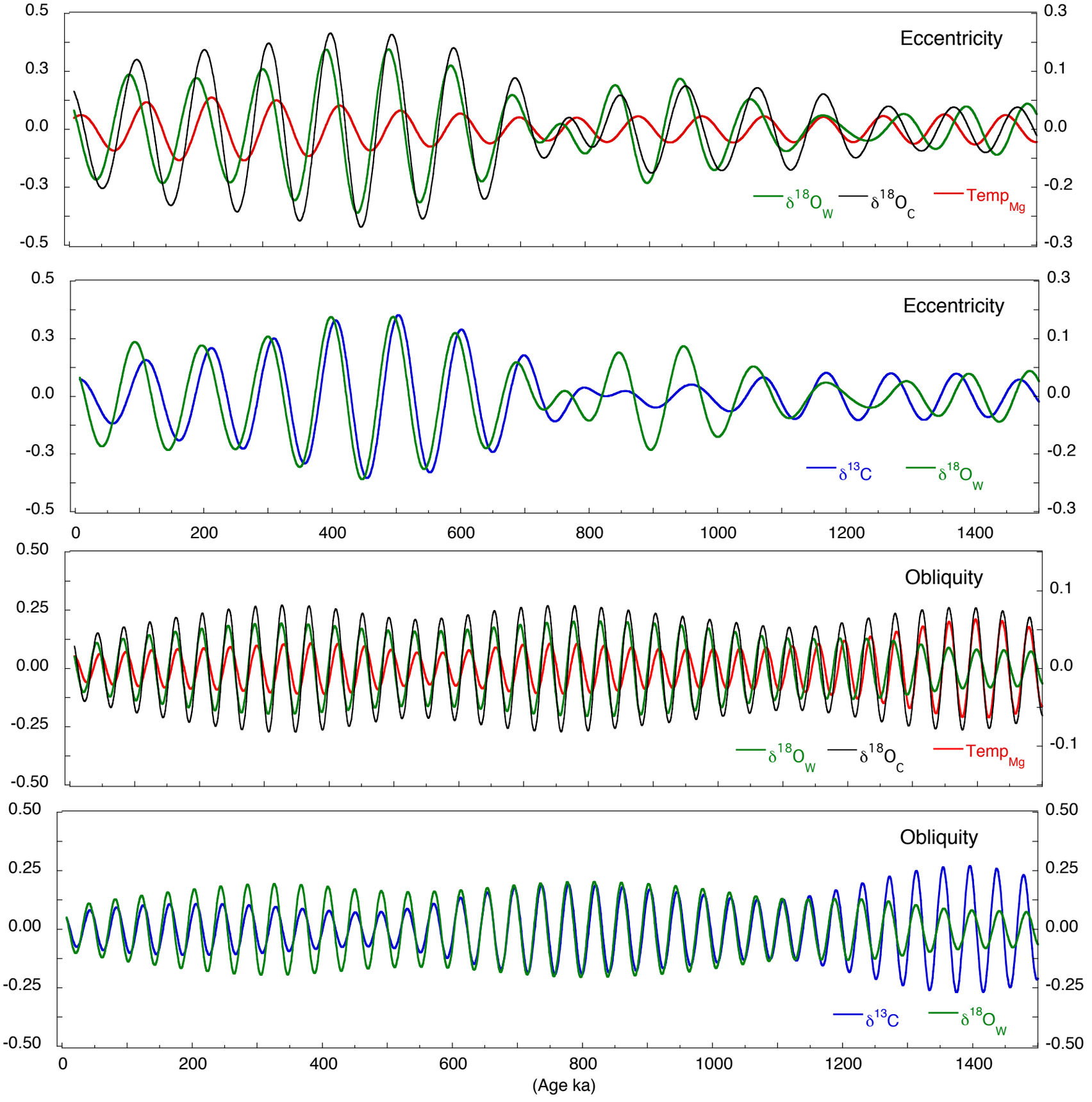
Eccentricity
δ18OW
δ18OC
TempMg
Eccentricity
δ13C
δ18OW
Obliquity
δ18OW
δ18OC
TempMg
Obliquity
δ13C
δ18OW
(Age ka)

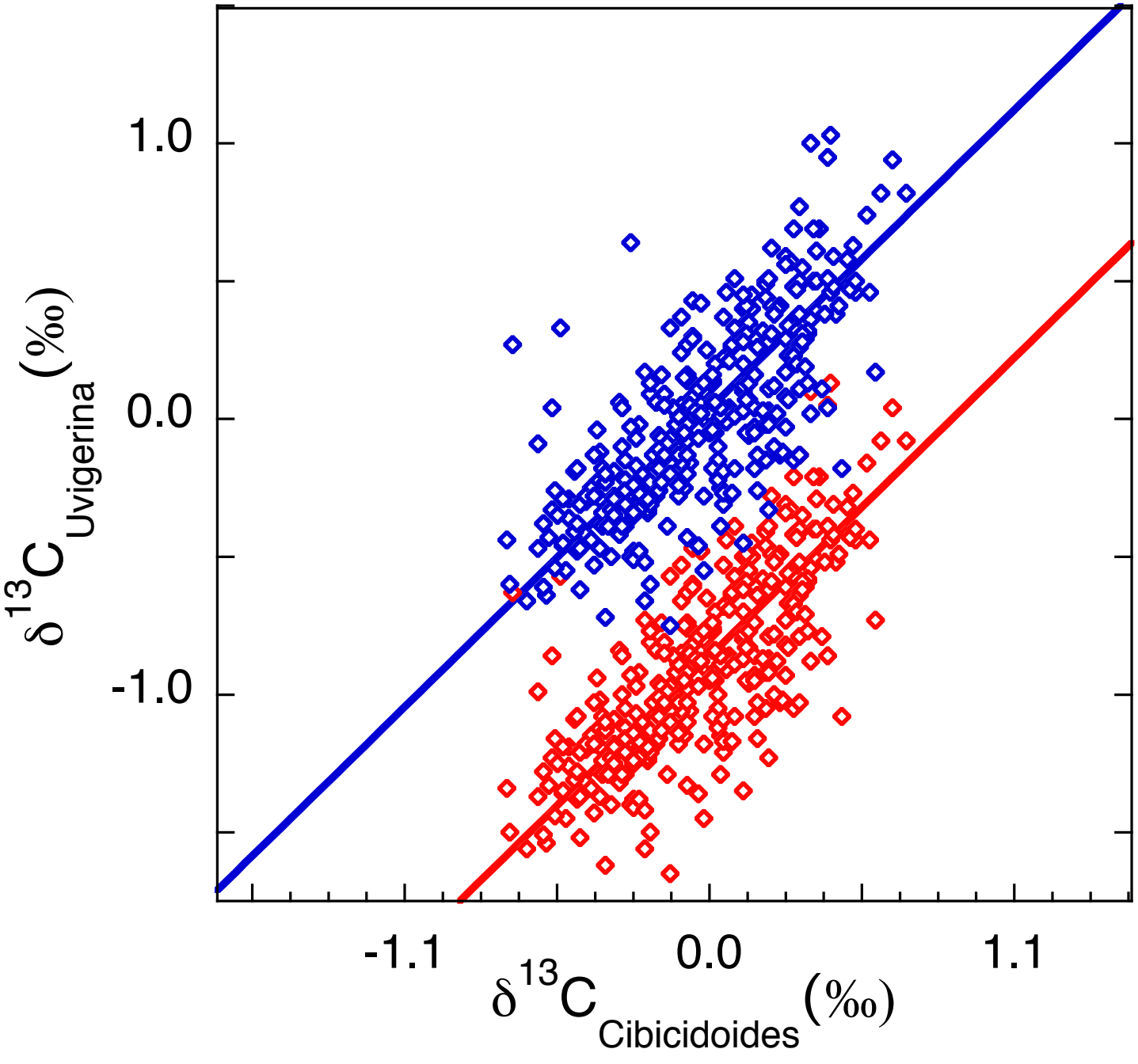
1.0
0.0
-1.0
-1.1
0.0
1.1
δ13CUvigerina (‰)
δ13CCibicidoides (‰)

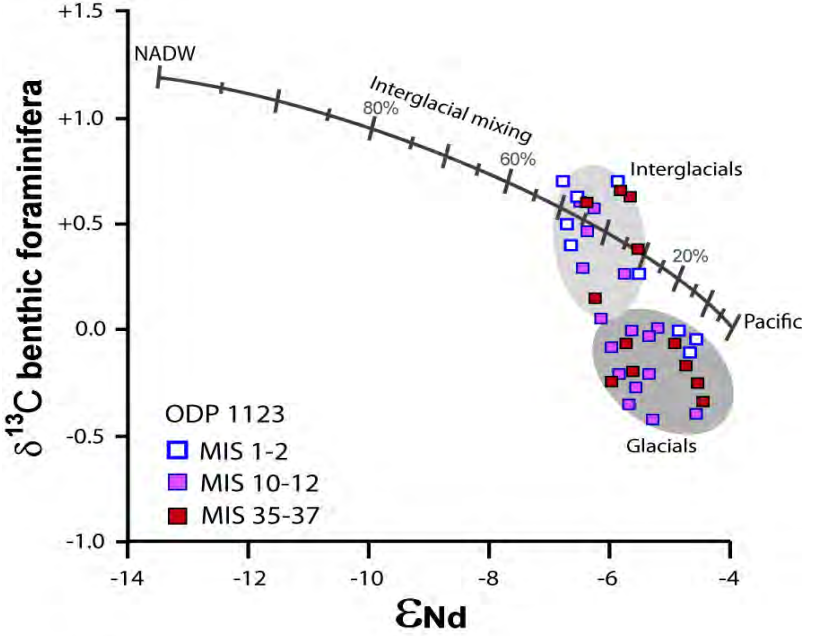
+1.5
+1.0
+0.5
0.0
-0.5
-1.0
δ13C benthic foraminifera
NADW
Interglacial mixing
80%
60%
20%
Interglacials
Pacific
Glacials
ODP 1123
MIS 1-2
MIS 10-12
MIS 35-37
-14
-12
-10
-8
-6
-4
εNd

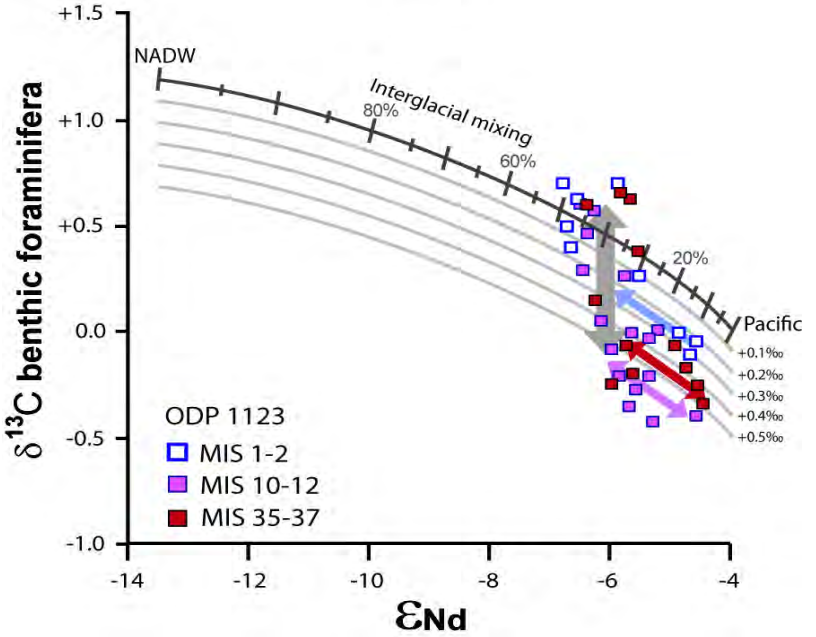
+1.5
+1.0
+0.5
0.0
-0.5
-1.0
δ13C benthic foraminifera
NADW
Interglacial mixing
80%
60%
20%
Pacific
+0.1‰
+0.2‰
+0.3‰
+0.4‰
+0.5‰
ODP 1123
MIS 1-2
MIS 10-12
MIS 35-37
-14
-12
-10
-8
-6
-4
εNd

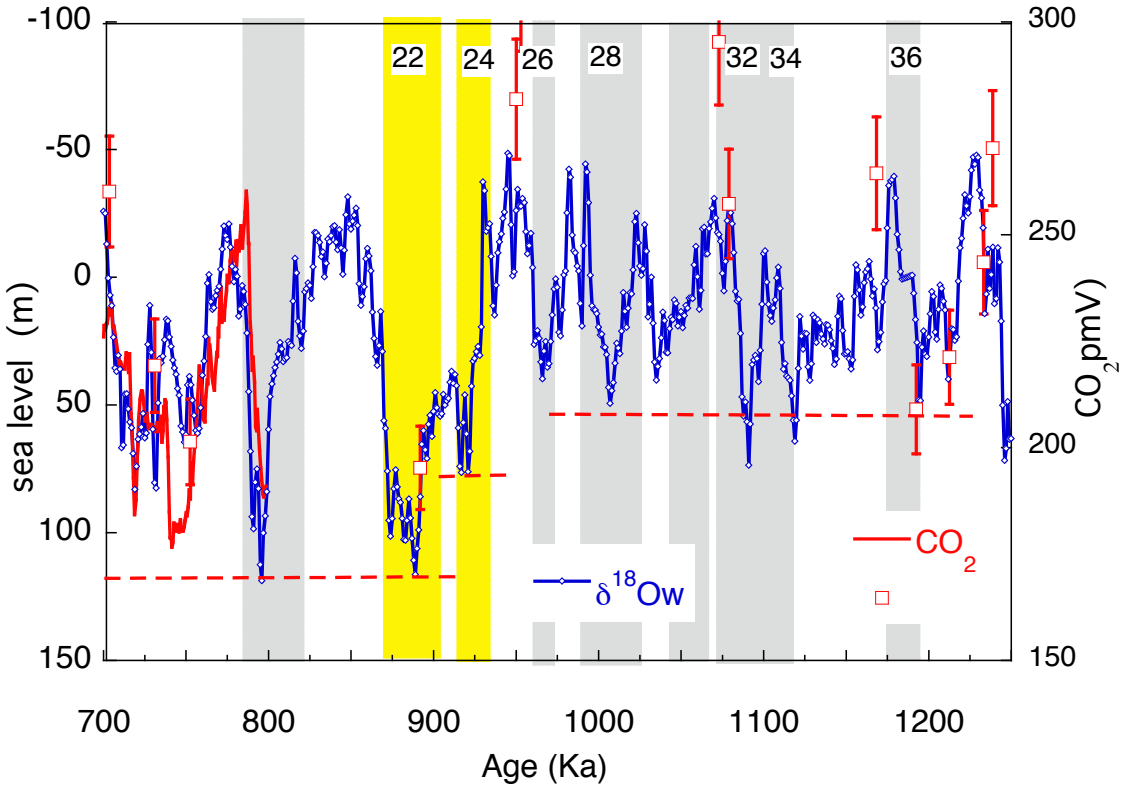
-100
-50
0
50
100
150
sea level (m)
300
250
200
150
CO2 pmV)
22
24
26
28
32
34
36
CO2
δ18Ow
700
800
900
1000
1100
1200
Age (Ka)

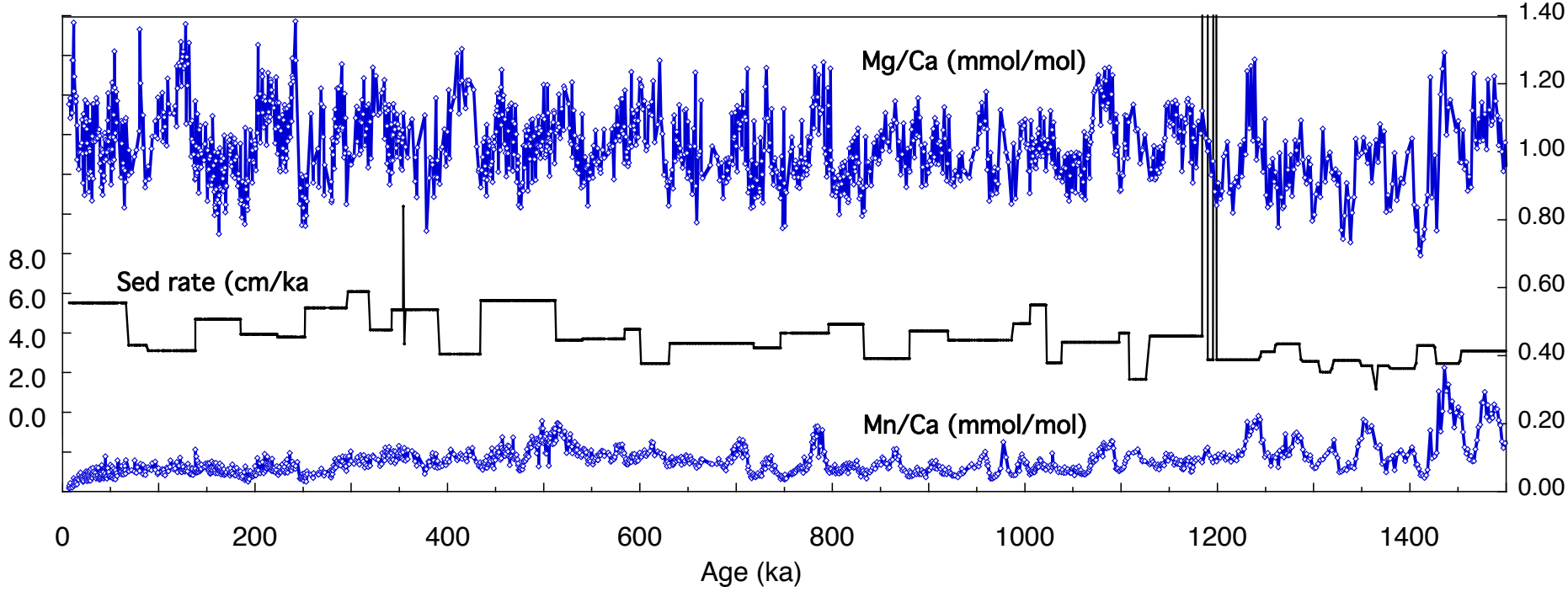
Mg/Ca (mmol/mol)
Sed rate (cm/ka
Mn/Ca (mmol/mol)
8.0
6.0
4.0
2.0
0.0
1.40
1.20
1.00
0.80
0.60
0.40
0.20
0.00
0
200
400
600
800
1000
1200
1400
Age (ka)

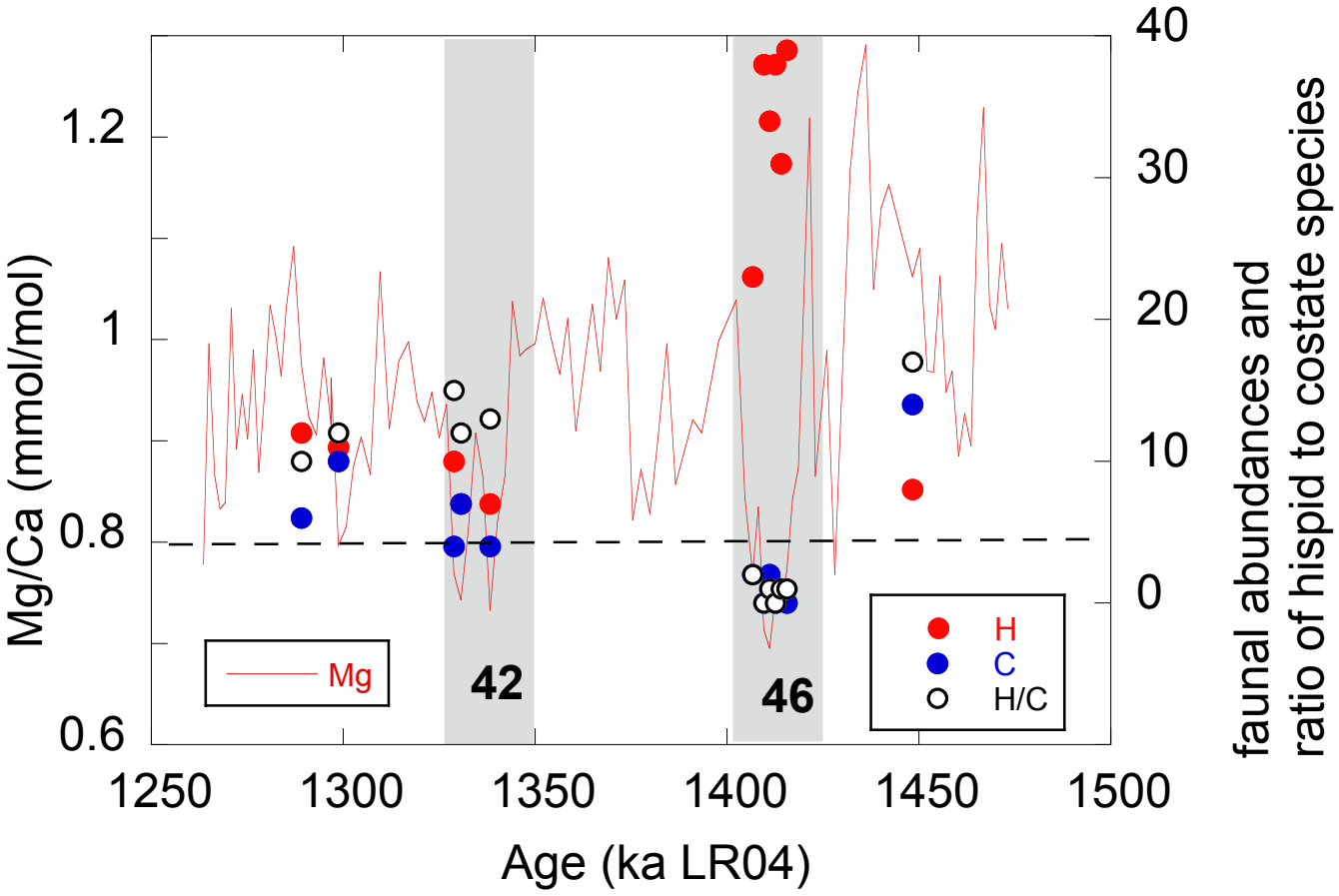
Mg/Ca (mmol/mol)
1.2
1
0.8
0.6
40
30
20
10
0
faunal abundances and
ratio of hispid to costate species
1250
1300
1350
1400
1450
1500
Age (ka LR04)
Mg
42
46
H
C
H/C

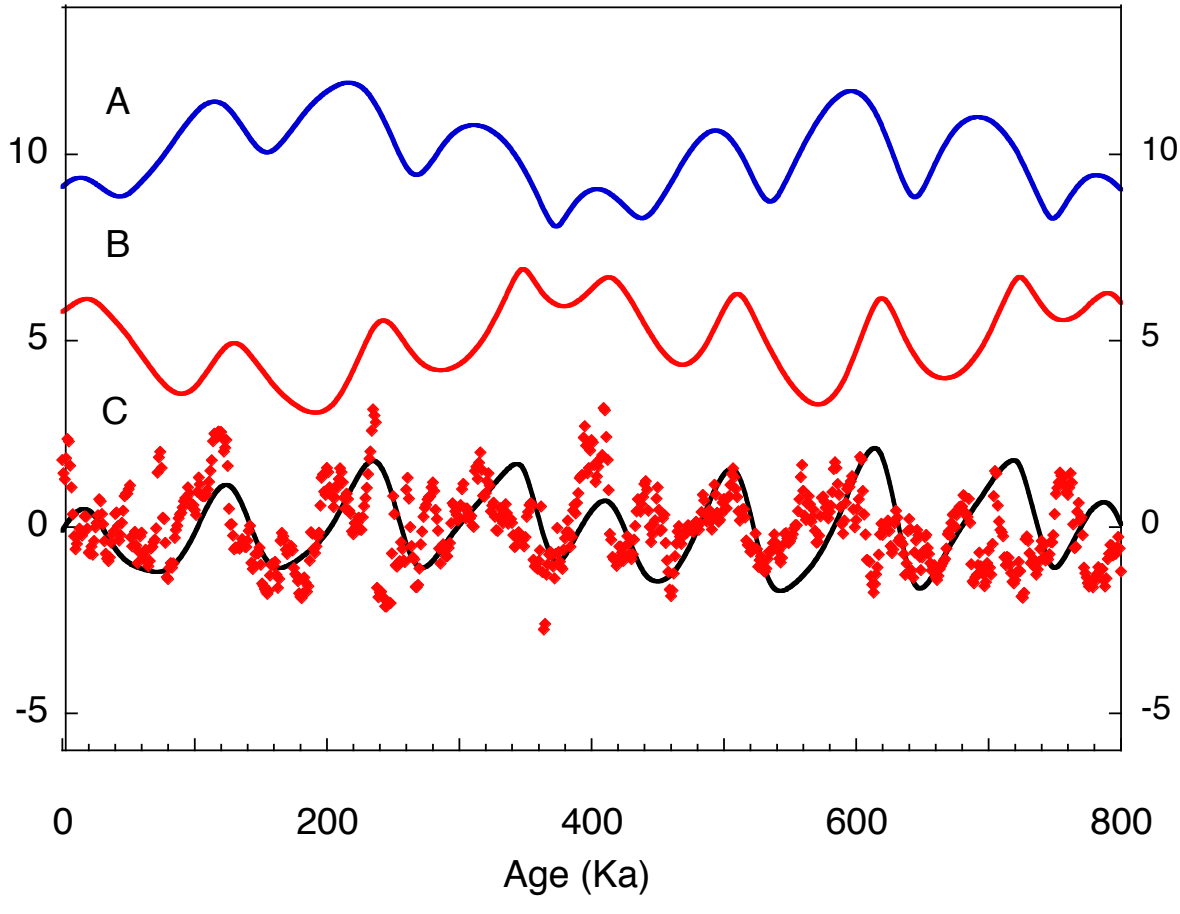
A
B
C
10
5
0
-5
0
200
400
600
800
Age (Ka)

Table S1 Sample metadata, Depth (revised m composite depth), age (LR04) *Uvigerina* spp. Mg/Ca $\delta^{18}O$, $\delta^{13}C$. Other data available at doi:10.1594/PANGAEA.786205.

Table S2 Duplicate analyses. 21 pairs of duplicates from archived data set, of which 20 are from the same depths down core from working (W) & archive (A) halves.

Table S3 "Cold samples" 18 samples having Mg/Ca <0.8 mmol/mol of which 6 have Mg/Ca < 0.75 mmol/mol. The samples are within a block of heavier individuals ~ 38 μg compared with ~26μg for typical samples

References

1. J. Chappell, N. J. Shackleton, Oxygen isotopes and sea level. *Nature* **324**, 137 (1986). doi:10.1038/324137a0

2. N. J. Shackleton, The 100,000-year ice-age cycle identified and found to lag temperature, carbon dioxide, and orbital eccentricity. *Science* **289**, 1897 (2000). doi:10.1126/science.289.5486.1897 Medline

3. N. J. Shackleton, Oxygen isotope analyses and Pleistocene temperatures re-assessed. *Nature* **215**, 15 (1967). doi:10.1038/215015a0

4. N. J. Shackleton, N. D. Opdyke, Oxygen isotope and paleomagnetic stratigraphy of Equatorial Pacific core V28–238: Oxygen isotope temperatures and ice volumes on a 105 and 106 year scale. *Quat. Res.* **3**, 39 (1973). doi:10.1016/0033-5894(73)90052-5

5. P. U. Clark *et al*., The Middle Pleistocene transition: Characteristics, mechanisms, and implications for long-term changes in atmospheric pCO_2. *Quat. Sci. Rev.* **25**, 3150 (2006). doi:10.1016/j.quascirev.2006.07.008

6. S. Sosdian, Y. Rosenthal, Deep-sea temperature and ice volume changes across the Pliocene-Pleistocene climate transitions. *Science* **325**, 306 (2009). doi:10.1126/science.1169938 Medline

7. P. A. Martin *et al*., Quaternary deep sea temperature histories derived from benthic foraminiferal Mg/Ca. *Earth Planet. Sci. Lett.* **198**, 193 (2002). doi:10.1016/S0012-821X(02)00472-7

8. H. Elderfield, J. Yu, P. Anand, T. Kiefer, B. Nyland, Calibrations for benthic foraminiferal Mg/Ca paleothermometry and the carbonate ion hypothesis. *Earth Planet. Sci. Lett.* **250**, 633 (2006). doi:10.1016/j.epsl.2006.07.041

9. J. Yu, W. S. Broecker, Comment on “Deep-sea temperature and ice volume changes across the Pliocene-Pleistocene climate transitions”. *Science* **328**, 1480 (2010). doi:10.1126/science.1186544 Medline

10. S. Sosdian, Y. Rosenthal, Response to Comment on “Deep-sea temperature and ice volume changes across the Pliocene-Pleistocene climate transitions”. *Science* **328**, 1480 (2010). doi:10.1126/science.1186768

11. R. Bintanja, R. S. W. van de Wal, J. Oerlemans, Modelled atmospheric temperatures and global sea levels over the past million years. *Nature* **437**, 125 (2005). doi:10.1038/nature03975 Medline

12. M. Siddall *et al*., Using a maximum simplicity paleoclimate model to simulate millennial variability during the last four glacial periods. *Quat. Sci. Rev.* **25**, 3185 (2006). doi:10.1016/j.quascirev.2005.12.014

13. E. M. Gasson *et al*., Exploring uncertainties in the relationship between temperature, ice volume, and sea level over the past 50 million years. *Rev. Geophys.* **50**, RG1005 (2012). doi:10.1029/2011RG000358

14. P. Kohler, H. Fischer, Simulating low frequency changes in atmospheric CO_2 during the last 740 000 years. *Clim. Past* **2**, 57 (2006). doi:10.5194/cp-2-57-2006

15. H. Elderfield *et al*., A record of bottom water temperature and seawater $\delta^{18}O$ for the Southern Ocean over the past 440 ka based on Mg/Ca of benthic foraminiferal Uvigerina spp. *Quat. Sci. Rev.* **29**, 160 (2010). doi:10.1016/j.quascirev.2009.07.013

16. J. Jouzel *et al*., Orbital and millennial Antarctic climate variability over the past 800,000 years. *Science* **317**, 793 (2007). doi:10.1126/science.1141038 Medline

17. I. N. McCave, L. Carter, I. R. Hall, Glacial–interglacial changes in water mass structure and flow in the SW Pacific Ocean. *Quat. Sci. Rev.* **27**, 1886 (2008). doi:10.1016/j.quascirev.2008.07.010

18. T. Whitworth, III *et al*., On the deep western-boundary current in the Southwest Pacific Basin. *Prog. Oceanogr.* **43**, 1 (1999). doi:10.1016/S0079-6611(99)00005-1

19. L. E. Lisiecki, M. E. Raymo, A Pliocene-Pleistocene stack of 57 globally distributed benthic $\delta^{18}O$ records. *Paleoceanography* **20**, PA1003 (2005). doi:10.1029/2004PA001071

20. F. Parrenin *et al*., The EDC3 chronology for the EPICA Dome C ice core. *Clim. Past* **3**, 485 (2007). doi:10.5194/cp-3-485-2007

21. A. Martínez-Garcia *et al*., Links between iron supply, marine productivity, sea surface temperature, and CO_2 over the last 1.1 Ma. *Paleoceanography* **24**, PA1207 (2009). doi:10.1029/2008PA001657

22. D. A. Hodell, K. A. Venz, C. D. Charles, F. J. Sierro, The mid-Brunhes transition in ODP sites 1089 and 1090, in *Earth's Climate and Orbital Eccentricity: The Marine Isotope Stage 11 Question*, A. W. Droxler, R. Z. Poore, L. H. Burckle, Eds., *AGU Geophys Monogr.* **137**, 113–129 (2003).

23. V. Masson-Delmotte *et al*., EPICA Dome C record of glacial and interglacial intensities. *Quat. Sci. Rev.* **29**, 113 (2010). doi:10.1016/j.quascirev.2009.09.030

24. W. G. Thompson, S. L. Goldstein, A radiometric calibration of the SPECMAP timescale: Application of the marine isotope stage stratigraphy. *Quat. Sci. Rev.* **25**, 3207 (2006). doi:10.1016/j.quascirev.2006.02.007

25. A. L. Thomas *et al*., Penultimate deglacial sea-level timing from uranium/thorium dating of Tahitian corals. *Science* **324**, 1186 (2009). doi:10.1126/science.1168754 Medline

26. J. F. Adkins, K. McIntyre, D. P. Schrag, The salinity, temperature, and $\delta^{18}O$ of the glacial deep ocean. *Science* **298**, 1769 (2002). doi:10.1126/science.1076252 Medline

27. A. Sima, A. Paul, M. Schulz, J. Oerlemans, Modeling the oxygen-isotopic composition of the North American Ice Sheet and its effect on the isotopic composition of the ocean during the last glacial cycle. *Geophys. Res. Lett.* **33**, L15706 (2006). doi:10.1029/2006GL026923

28. M. Siddall *et al*., Sea-level fluctuations during the last glacial cycle. *Nature* **423**, 853 (2003). doi:10.1038/nature01690 Medline

29. D. Maraun, J. Kurths, M. Holschneider, Nonstationary Gaussian processes in wavelet domain: synthesis, estimation, and significance testing. *Phys. Rev. E Stat. Nonlin. Soft Matter Phys.* **75**, 016707 (2007). doi:10.1103/PhysRevE.75.016707 Medline

30. D. Maraun, J. Kurths, Cross wavelet analysis: Significance testing and pitfalls. *Nonlin. Processes Geophys.* **11**, 505 (2004). doi:10.5194/npg-11-505-2004

31. D. Paillard, The timing of Pleistocene glaciations from a simple multiple-state climate model. *Nature* **391**, 378 (1998). doi:10.1038/34891

32. P. D. Ditlevsen, Bifurcation structure and noise-assisted transitions in the Pleistocene glacial cycles. *Paleoceanography* **24**, PA3204 (2009). doi:10.1029/2008PA001673

33. K. T. Lawrence, S. Sosdian, H. E. White, Y. Rosenthal, North Atlantic climate evolution through the Plio-Pleistocene climate transitions. *Earth Planet. Sci. Lett.* **300**, 329 (2010). doi:10.1016/j.epsl.2010.10.013

34. M. E. Raymo, L. E. Lisiecki, K. H. Nisancioglu, Plio-Pleistocene ice volume, Antarctic climate, and the global $\delta^{18}O$ record. *Science* **313**, 492 (2006). doi:10.1126/science.1123296 Medline

35. T. Naish *et al*., Obliquity-paced Pliocene West Antarctic ice sheet oscillations. *Nature* **458**, 322 (2009). doi:10.1038/nature07867 Medline

36. D. Pollard, R. M. DeConto, Modelling West Antarctic ice sheet growth and collapse through the past five million years. *Nature* **458**, 329 (2009). doi:10.1038/nature07809 Medline

37. R. McKay *et al*., Pleistocene variability of Antarctic Ice Sheet extent in the Ross Embayment. *Quat. Sci. Rev.* **34**, 93 (2012). doi:10.1016/j.quascirev.2011.12.012

38. M. E. Raymo, D. W. Oppo, W. Curry, The mid-Pleistocene climate transition: a deep-sea carbon isotopic perspective. *Paleoceanography* **12**, 546 (1997). doi:10.1029/97PA01019

39. D. A. Hodell, K. A. Venz, C. D. Charles, U. S. Ninneman, Pleistocene vertical carbon isotope and carbonate gradients in the South Atlantic sector of the Southern Ocean. *Geochem. Geophys. Geosyst.* **4**, 1004 (2003). doi:10.1029/2002GC000367

40. L. E. Lisiecki, A benthic $\delta^{13}C$-based proxy for atmospheric pCO_2 over the last 1.5 Myr. *Geophys. Res. Lett.* **37**, L21708 (2010). doi:10.1029/2010GL045109

41. P. Wang, J. Tian, L. J. Lourens, Obscuring of long eccentricity cyclicity in Pleistocene oceanic carbon isotope records. *Earth Planet. Sci. Lett.* **290**, 319 (2010). doi:10.1016/j.epsl.2009.12.028

42. B. A. A. Hoogakker, E. J. Rohling, M. R. Palmer, T. Tyrrell, R. G. Rothwell, Underlying causes for long-term global ocean $\delta^{13}C$ fluctuations over the last 1.20 Myr. *Earth Planet. Sci. Lett.* **248**, 15 (2006). doi:10.1016/j.epsl.2006.05.007

43. K. A. Venz, D. A. Hodell, New evidence for changes in Plio-Pleistocene deep water circulation from Southern Ocean ODP leg 177 site 1090. *Palaeogeogr. Palaeoclimatol. Palaeoecol.* **182**, 197 (2002). doi:10.1016/S0031-0182(01)00496-5

44. N. J. Shackleton, Tropical rainforest history and the equatorial Pacific carbonate dissolution cycles. In *Fate of Fossil Fuel CO_2 in the Oceans*, N. R. Anderson, A. Malahoff, Eds. (Plenum, New York, 1977) pp. 401-427.

45. I. R. Hall, I. N. McCave, N. J. Shackleton, G. P. Weedon, S. E. Harris, Intensified deep Pacific inflow and ventilation in Pleistocene glacial times. *Nature* **412**, 809 (2001). doi:10.1038/35090552 Medline

46. A. M. Piotrowski, S. L. Goldstein, S. R. Hemming, R. G. Fairbanks, Temporal relationships of carbon cycling and ocean circulation at glacial boundaries. *Science* **307**, 1933 (2005). doi:10.1126/science.1104883 Medline

47. B. Hönisch, N. G. Hemming, D. Archer, M. Siddall, J. F. McManus, Atmospheric carbon dioxide concentration across the mid-Pleistocene transition. *Science* **324**, 1551 (2009). doi:10.1126/science.1171477 Medline

48. S. Barker, M. Greaves, H. Elderfield, A study of cleaning procedures used for foraminiferal Mg/Ca paleothermometry. *Geochem. Geophys. Geosyst.* **4**, 8407 (2003). doi:10.1029/2003GC000559

49. S. de Villiers, M. J. Greaves, H. Elderfield, An intensity ratio calibration method for the accurate determination of Mg/Ca and Sr/Ca of marine carbonates by ICP-AES. *Geochem. Geophys. Geosyst.* **3**, GC000169 (2002). doi:10.1029/2001GC000169

50. J. Yu, J. Day, M. J. Greaves, H. Elderfield, Determination of multiple element/calcium ratios in foraminiferal calcite by quadrupole ICP-MS. *Geochem. Geophys. Geosyst.* **6**, Q08P01 (2005). doi:10.1029/2005GC000964

51. Y. Rosenthal *et al*., Interlaboratory comparison study of Mg/Ca and Sr/Ca measurements in planktonic foraminifera for paleoceanographic research. *Geochem. Geophys. Geosyst.* **5**, Q04D09 (2004). doi:10.1029/2003GC000650

52. M. Greaves *et al*., Interlaboratory comparison study of calibration standards for foraminiferal Mg/Ca thermometry. *Geochem. Geophys. Geosyst.* **9**, Q08010 (2008). doi:10.1029/2008GC001974

53. G. J. de Lange, B. Vanos, R. Poorter, Geochemical composition and inferred accretion rates of sediments and manganese nodules from a submarine hill in the Madeira Abyssal Plain, Eastern North Atlantic. *Mar. Geol.* **109**, 171 (1992). doi:10.1016/0025-3227(92)90227-9

54. J. N. Pattan, Manganese micronodules: A possible indicator of sedimentary environments. *Mar. Geol.* **113**, 331 (1993). doi:10.1016/0025-3227(93)90026-R

55. T. F. Pederson, N. B. Price, The geochemistry of manganese carbonate in Panama Basin sediments. *Geochim. Cosmochim. Acta* **46**, 59 (1982). doi:10.1016/0016-7037(82)90290-3

56. S. E. Harris, Data report: Late Pliocene–Pleistocene carbon and oxygen stable isotopes from benthic foraminifers at Ocean Drilling Program site 1123 in the Southwest Pacific. In Richter, C. (Ed.), *Proc. ODP, Sci. Results*, 181, 1-20 (2002).

57. A. S. R. Allan, J. A. Baker, L. Carter, R. J. Wysoczanksi, Reconstructing the Quaternary evolution of the world's most active silicic volcanic system: insights from an ~1.65 Ma deep ocean tephra record sourced from Taupo Volcanic Zone, New Zealand. *Quat. Sci. Rev.* **27**, 2341 (2008). doi:10.1016/j.quascirev.2008.09.003

58. T. Tanaka *et al*., JNdi-1: a neodymium isotopic reference in consistency with LaJolla neodymium. *Chem. Geol.* **168**, 279 (2000). doi:10.1016/S0009-2541(00)00198-4

59. W. F. Ruddiman, Orbital insolation, ice volume, and greenhouse gases. *Quat. Sci. Rev.* **22**, 1597 (2003). doi:10.1016/S0277-3791(03)00087-8

60. L. E. Lisiecki, Links between eccentricity forcing and the 100,000-year glacial cycle. *Nat. Geosci.* **3**, 349 (2010). doi:10.1038/ngeo828

61. N. J. Shackleton, A. Berger, W. R. Peltier, An alternative astronomical calibration of the lower Pleistocene time scale based on ODP site 677. *Trans. R. Soc. Edinb. Earth Sci.* **81**, 251 (1990). doi:10.1017/S0263593300020782

62. A. C. Mix, J. Le, N. J. Shackleton, Benthic foraminiferal stable isotope stratigraphy of site 846: 0–1.8 Ma, in N. G. Pisias, L. A. Mayer, T. R. Janecek, A. Palmer-Julson, T. H. van Andel, Eds., *Proc. ODP, Sci. Results, 138*: College Station, TX (Ocean Drilling Program) (1995), pp. 839–854.

63. D. A. Hodell *et al*., Data report: oxygen isotope stratigraphy of ODP leg 177 sites 1088, 1089, 1090, 1093, and 1094, in R. Gersonde, D. A. Hodell, P. Blum, Eds., *Proc. ODP, Sci. Results, 177*: College Station, TX (Ocean Drilling Program), 1–26 (2003), doi:10.2973/odp.proc.sr.177.120.2003

64. D. A. Hodell, J. E. T. Channell, J. H. Curtis, O. E. Romero, U. Röhl, Onset of "Hudson Strait" Heinrich events in the eastern North Atlantic at the end of the middle Pleistocene transition (~640ka)? *Paleoceanography* **23**, PA4218 (2008). doi:10.1029/2008PA001591